

# When Cloud Removal Meets Diffusion Model in Remote Sensing

Zhenyu Yu<sup>2</sup>, Mohd Yamani Idna Idris<sup>2</sup>, Pei Wang<sup>1,\*</sup>

<sup>1</sup>Kunming University of Science and Technology

<sup>2</sup>Universiti Malaya

yuzhenyuyxl@foxmail.com, yamani@um.edu.my, peiwan@kust.edu.cn

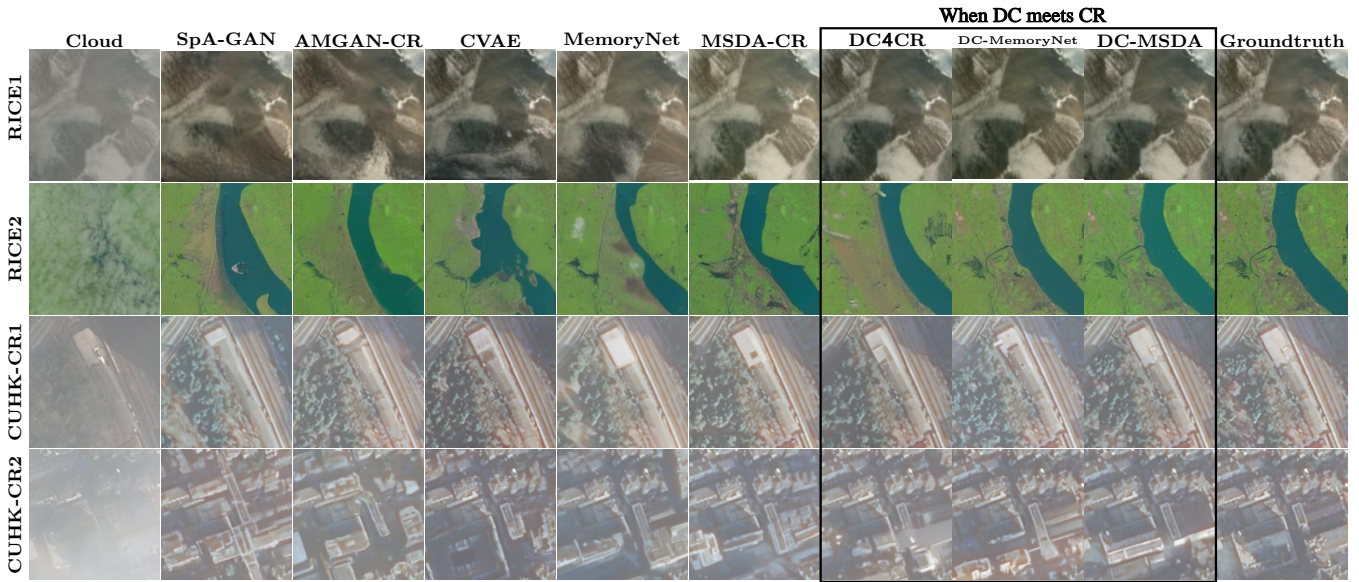


Figure 1: Model comparison results. It indicates that our DC4CR model and other variants (DC-memorynet and DC-MSDA) excel across all conventional models. Note that these images can zoom in images, and the original images are shown in A.2.

## Abstract

Cloud occlusion significantly hinders remote sensing applications by obstructing surface information and complicating analysis. To address this, we propose **DC4CR** (Diffusion Control for Cloud Removal), a novel multimodal diffusion-based framework for cloud removal in remote sensing imagery. Our method introduces prompt-driven control, allowing selective removal of thin and thick clouds without relying on pre-generated cloud masks, thereby enhancing preprocessing efficiency and model adaptability. Additionally, we integrate low-rank adaptation for computational efficiency, subject-driven generation for improved generalization, and grouped learning to enhance performance on small datasets. Designed as a plug-and-play module, DC4CR seamlessly integrates into existing cloud removal models, providing a scalable and robust solution. Extensive experiments on the RICE and CUHK-CR datasets demonstrate state-of-the-

art performance, achieving superior cloud removal across diverse conditions. This work presents a practical and efficient approach for remote sensing image processing with broad real-world applications.

## 1 Introduction

High-resolution multispectral remote sensing has significantly advanced Earth observation, enabling precise analysis of land cover, vegetation health, urban development, and environmental changes Yu *et al.* [2023]; Tan *et al.* [2023]. However, cloud cover remains a major challenge in remote sensing image analysis, obstructing surface information and introducing uncertainty, particularly in multimodal datasets where different cloud formations increase restoration complexity [Zi *et al.*, 2018; Irons *et al.*, 2012; Yang *et al.*, 2020]. Thus, efficient cloud removal is a crucial preprocessing step for applications such as agriculture monitoring, disaster assessment, and land-use classification.

Cloud removal aims to reconstruct cloud-covered regions while preserving spatial and spectral consistency. **Physical model-based methods** rely on atmospheric correction and spectral analysis to detect and remove clouds [Hu *et al.*, 2015; Yu and Wang, 2024; Wang *et al.*, 2024b]. While effective for thin clouds, these methods struggle with complex cloud structures and varying atmospheric conditions, often failing to reconstruct occluded surface details [Xu *et al.*, 2019; Yu and Chan, 2025]. **Deep learning-based methods** have shown promising results by learning cloud removal patterns from large-scale datasets [Pan, 2020; Xu *et al.*, 2022; Yu *et al.*, 2025b]. Techniques such as convolutional neural networks (CNNs), generative adversarial networks (GANs), and variational autoencoders (VAEs) have been employed to enhance cloud removal accuracy. However, these models often lack adaptability to different cloud types and face challenges in generalizing to small dataset scenarios, limiting their robustness in real-world applications [Ebel *et al.*, 2022; Yu *et al.*, 2025a]. **Multimodal approaches** integrate optical imagery with synthetic aperture radar (SAR) to exploit the complementary characteristics of different sensors [Xu *et al.*, 2019; Pan, 2020; Yu, 2025]. These methods improve cloud removal performance by leveraging SAR’s ability to penetrate clouds, but they require precise data alignment and registration, which remains a significant challenge for large-scale deployment [Ebel *et al.*, 2022; Xu *et al.*, 2022].

Recently, **diffusion models** have emerged as a powerful paradigm for image restoration due to their iterative refinement capabilities [Ho *et al.*, 2020; Yang *et al.*, 2025], enabling the progressive reconstruction of missing or occluded regions through structured noise removal, making them well-suited for cloud removal tasks. However, directly applying diffusion models to cloud removal presents several challenges. First, adaptability to different cloud types remains a significant issue, as most existing methods employ a uniform restoration approach for both thin and thick clouds, often resulting in incomplete removal of thick clouds or excessive removal of thin clouds, thereby distorting surface details. Second, the high computational cost of diffusion models poses a practical limitation, as they require multiple denoising iterations, making them computationally expensive and impractical for large-scale remote sensing applications. Lastly, inconsistent color restoration after cloud removal is another major drawback, as existing methods often fail to preserve color consistency in reconstructed images, leading to mismatches or artifacts across different regions, ultimately affecting both visual quality and the performance of downstream tasks.

**Limitations of existing methods.** Despite advancements in cloud removal, current approaches still face fundamental challenges. One major limitation is the lack of a unified framework for different cloud types, as most methods treat thin and thick clouds separately, necessitating additional model training or preprocessing steps, thereby increasing complexity. Additionally, computational inefficiency remains a concern, particularly with diffusion models, which, despite their high restoration quality, require a multi-step denoising process that incurs substantial computational costs, making them difficult to scale for real-world applications. Furthermore, color inconsistencies after cloud removal often degrade

visual quality and usability, as existing methods frequently fail to maintain color consistency between restored and surrounding areas, leading to mismatched tones that can negatively impact subsequent remote sensing analysis.

To address these challenges, we propose **Diffusion Control for Cloud Removal (DC4CR)**, a novel multimodal diffusion framework that introduces prompt-driven controllability for efficient and adaptive cloud removal. Our main **contributions** are:

- **Prompt-based controllable cloud removal.** We introduce a prompt-driven control mechanism that enables a unified framework for removing both thin and thick clouds. Unlike prior methods that require separate models for different cloud types, our approach allows users to flexibly control cloud removal effects via prompt adjustments, enhancing adaptability across diverse cloud conditions.
- **Efficient diffusion-based cloud removal with Low-Rank Adaptation and Grouped Learning.** To reduce computational costs, we integrate Low-Rank Adaptation (LoRA) for efficient fine-tuning and Grouped Learning for progressive training. LoRA updates only a subset of parameters, while Grouped Learning enhances generalization by gradually increasing task complexity. These optimizations improve efficiency, enabling DC4CR to scale for large-scale remote sensing applications.
- **Image color optimization for enhanced consistency.** We integrate a VGG-19 module with Gram matrix constraints to improve color consistency. VGG-19 extracts style features for natural color restoration, while Gram matrices ensure uniform color distribution. This reduces color shifts and artifacts, enhancing the visual quality of remote sensing imagery.

## 2 Related Work

### 2.1 Traditional Cloud Removal Methods

**Multispectral methods** leverage wavelength-dependent absorption and reflection to reconstruct occluded landscapes [Xu *et al.*, 2019], but they struggle with thick clouds that completely block optical signals [Hu *et al.*, 2015]. **Multitemporal methods** mitigate this issue by integrating cloud-free reference images captured at different times [Chen *et al.*, 2019]. However, these methods heavily depend on the availability of clear-sky images, making them less effective in dynamic weather conditions.

**Other conventional approaches**, including interpolation [Ebel *et al.*, 2022], wavelet transforms [Ji *et al.*, 2020], and information cloning [Pan, 2020], have been explored to reconstruct cloud-contaminated regions. Additionally, sparse representation-based methods [Xu *et al.*, 2022], low-pass filtering [Rombach *et al.*, 2022], and dictionary learning [Li *et al.*, 2014] have been investigated.

Despite their effectiveness in certain scenarios, traditional methods generally fail to handle **diverse cloud types within a unified framework**. They often struggle with thick clouds, require manual intervention, and lack robustness in complex

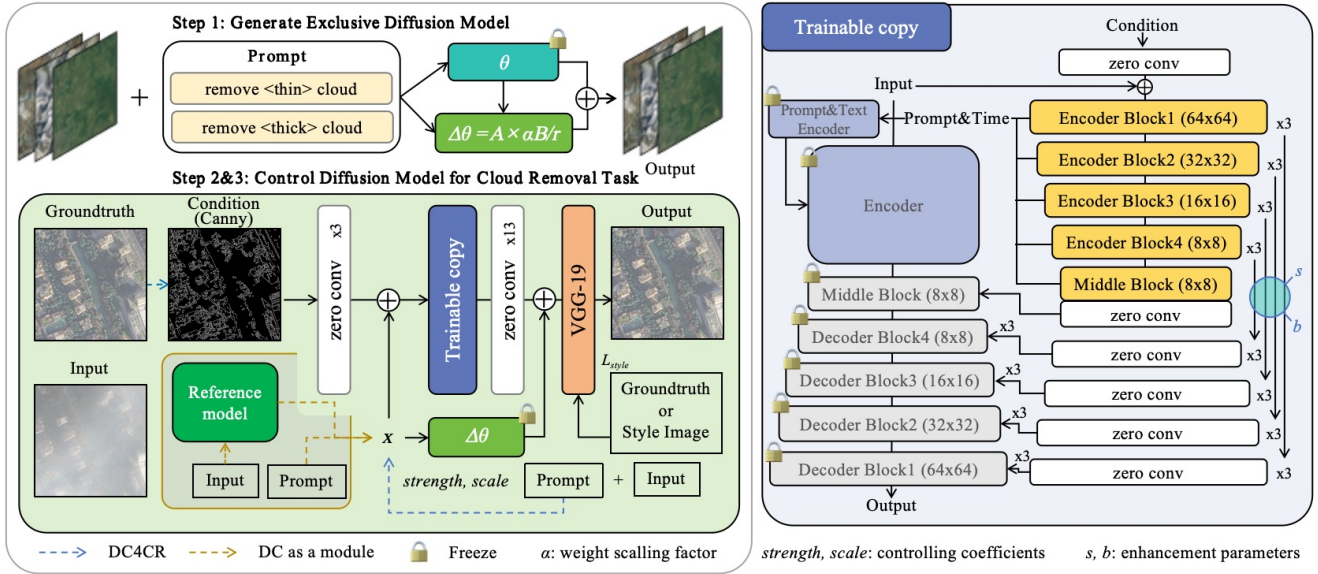


Figure 2: Overall workflow of the diffusion control for cloud removal (DC4CR) in remote sensing images. It illustrates the three main steps of the diffusion model designed for cloud removal tasks. **Step 1:** The text-to-image diffusion model is fine-tuned using prompts tailored to remote sensing characteristics to enhance the model’s understanding and accuracy in generating remote sensing images. **Step 2 & 3:** The cloud removal task is implemented by allowing users to select specific conditions to efficiently remove clouds and restore clear surface information. Meanwhile, optimize the quality of generated image.

atmospheric conditions. These limitations have led to the adoption of deep learning-based approaches.

## 2.2 Deep Learning-Based Cloud Removal

Deep learning models have significantly improved CR performance by learning complex cloud removal patterns from large-scale datasets.

**Generative models**, such as GANs and VAEs, have been widely adopted. SpA-GAN and AMGAN-CR employ spatial attention mechanisms to enhance cloud removal accuracy [Pan, 2020; Xu *et al.*, 2022], while CVAE introduces uncertainty modeling for improved robustness [Ding *et al.*, 2022]. However, these methods often struggle with **thick cloud occlusion**, leading to texture inconsistencies and loss of fine details.

**Memory-augmented architectures**, such as MemoryNet [Zhang *et al.*, 2023b] and MSDA-CR [Yu *et al.*, 2022], integrate multiscale learning to improve structural consistency. Despite their effectiveness, these approaches require **significant computational resources**, making real-time processing challenging.

Furthermore, most deep learning-based methods **lack adaptability** to different cloud types and require explicit cloud masks, which introduce additional preprocessing complexity. To overcome these issues, more flexible and computationally efficient models are needed.

## 2.3 Diffusion Models for Cloud Removal

Diffusion models have emerged as powerful frameworks for image synthesis, video generation, and high-fidelity restoration [Saharia *et al.*, 2022; Ho *et al.*, 2022; Kawar *et al.*, 2023]. Unlike traditional deep learning-based CR models,

diffusion models iteratively refine images through noise removal, making them particularly effective in reconstructing cloud-occluded regions [Ho *et al.*, 2020].

In remote sensing, IDF-CR pioneered the application of diffusion models for CR by combining pixel-wise cloud reconstruction with iterative refinement [Wang *et al.*, 2024a]. Similarly, the DE method integrates reference priors to balance image fusion and employs a coarse-to-fine strategy for faster convergence [Sui *et al.*, 2024]. However, existing diffusion-based methods remain **computationally expensive** due to their multiple denoising iterations, limiting their scalability for large-scale applications.

Additionally, most current diffusion models **apply uniform reconstruction strategies**, making it difficult to adapt to varying cloud types. Since cloud removal often introduces **color inconsistencies and artifacts**, a more controlled and adaptable diffusion process is required.

## 3 Method

### 3.1 Model Overview

This paper presents **DC4CR**, a diffusion-based framework for cloud removal in remote sensing imagery (see Figure 2). The model consists of three main components:

**Step 1: Text-to-Image Diffusion Model.** We fine-tune the Stable Diffusion model on remote sensing images using controlled prompts to ensure the generation of high-quality cloud-free imagery.

**Step 2: Cloud Removal via Controlled Diffusion.** By leveraging diffusion control mechanisms, we enable flexible cloud removal under different conditions (e.g., cloud thickness and type), achieving precise surface reconstruction.

Table 1: Comparison of cloud removal performance. Our model demonstrates superior results compared to other models.

Method	RICE1			RICE2			CUHK-CR1			CUHK-CR2		
	PSNR↑	SSIM↑	LPIPS↓									
SpA-GAN	28.509	0.9122	0.0503	28.783	0.7884	0.0963	20.999	0.5162	0.0830	19.680	0.3952	0.1201
AMGAN-CR	26.497	0.912	0.0447	28.336	0.7819	0.1105	20.867	0.4986	0.1075	20.172	0.4900	0.0932
CVAE	31.112	0.9733	0.0149	30.063	0.8474	0.0743	24.252	0.7252	0.1075	22.631	0.6302	0.0489
MemoryNet	34.427	0.9865	0.0067	32.889	0.8801	0.0557	26.073	0.7741	0.0315	24.224	0.6838	0.0403
MSDA-CR	34.569	0.9871	0.0073	33.166	0.8793	0.0463	25.435	0.7483	0.0374	23.755	0.6661	0.0433
DE-MemoryNet	35.525	0.9882	0.0055	33.637	0.8825	0.0476	26.183	0.7746	0.0290	24.348	0.6843	0.0369
DE-MSDA	35.357	0.9878	0.0061	33.598	0.8842	0.0452	25.739	0.7592	0.0321	23.968	0.6737	0.0372
DC4CR	<b>35.542</b>	<b>0.9887</b>	<b>0.0054</b>	<b>33.678</b>	<b>0.8859</b>	<b>0.0451</b>	<b>26.291</b>	<b>0.7790</b>	<b>0.0285</b>	<b>24.595</b>	<b>0.6986</b>	<b>0.0326</b>

Table 2: Grouped training results. It includes the impact of ungrouped, 2-group, and 3-group training on model performance.

Group	RICE1			RICE2			CUHK-CR1			CUHK-CR2		
	PSNR↑	SSIM↑	LPIPS↓	PSNR↑	SSIM↑	LPIPS↓	PSNR↑	SSIM↓	LPIPS↓	PSNR↑	SSIM↑	LPIPS↓
No grouping	35.535	0.9882	0.0056	33.670	0.8840	0.0458	26.284	0.7736	0.0291	24.594	0.6911	0.0331
2 Groups	35.538	0.9866	0.0062	33.676	0.8789	0.0455	26.288	0.7783	0.0289	24.586	0.6936	0.0331
3 Groups	<b>35.542</b>	<b>0.9887</b>	<b>0.0054</b>	<b>33.678</b>	<b>0.8859</b>	<b>0.0451</b>	<b>26.291</b>	<b>0.7790</b>	<b>0.0285</b>	<b>24.595</b>	<b>0.6986</b>	<b>0.0326</b>

*Step 3: Optimization and Modularization.* We incorporate FreeU to refine image quality and introduce a modular structure to enhance adaptability and generalization in complex remote sensing scenarios.

### 3.2 Generating Remote Sensing Diffusion Model

**Prompt Selection.** To enable adaptive cloud removal, we categorize clouds into two types: thin and thick. Prompt-based control is applied to condition the diffusion process using training directives such as:

remove <thin / thick> cloud.

These prompts guide the model in recognizing different cloud characteristics and generating high-fidelity cloud-free outputs.

**Low-Rank Adaptation (LoRA).** To efficiently fine-tune the Stable Diffusion model for cloud removal, we employ LoRA [Hu *et al.*, 2021], which introduces low-rank decomposition to reduce computational cost while maintaining adaptation flexibility. The updated model parameters are defined as:

$$\theta_l = \theta + \frac{\alpha}{r} \mathbf{A}\mathbf{B}, \quad (1)$$

where  $\theta$  represents the original model parameters,  $\mathbf{A} \in \mathbb{R}^{m \times k}$  and  $\mathbf{B} \in \mathbb{R}^{k \times n}$  are low-rank matrices with  $k \ll \min(m, n)$ , and  $\alpha$  is a scaling factor regulating adaptation strength. The term  $r$  represents the rank of the low-rank decomposition, controlling the dimensionality reduction of the weight update.

During training, only  $\mathbf{A}$  and  $\mathbf{B}$  are updated while keeping  $\theta$  frozen, allowing efficient domain adaptation without overwriting pre-trained knowledge:

$$\Delta\theta = \frac{\alpha}{r} \mathbf{A}\mathbf{B}. \quad (2)$$

By setting  $r$  appropriately, the model balances expressiveness and computational efficiency, reducing memory consumption while maintaining adaptation capability for small remote sensing datasets.

**Subject-Driven Generation.** To enhance model adaptability to diverse cloud structures, we employ DreamBooth [Ruiz *et al.*, 2023] for fine-tuning, using a combination of real and synthesized images to refine the diffusion process. Given a cloud-covered input image  $\mathbf{x}$ , the model learns a domain-specific prior  $p(\mathbf{x})$  conditioned on subject-specific embeddings  $\mathbf{z}_s$ , ensuring accurate cloud removal while preserving structural details. The objective function is formulated as:

$$\mathcal{L} = \lambda_1 \|\mathbf{x} - \mathbf{x}'\|^2 + \lambda_2 \cdot \text{SSIM}(\mathbf{x}, \mathbf{x}'), \quad (3)$$

where  $\mathbf{x}'$  represents the generated cloud-free image, and  $\lambda_1, \lambda_2$  are weighting factors balancing pixel-wise accuracy and perceptual similarity.

To improve image quality, we iteratively update the latent representation  $\mathbf{z}_s$  while keeping most pre-trained parameters frozen:

$$\mathbf{z}_s^{(t+1)} = \mathbf{z}_s^{(t)} - \eta \nabla_{\mathbf{z}_s} \mathcal{L}, \quad (4)$$

where  $\eta$  is the learning rate. This process ensures high-fidelity reconstruction while maintaining structural and textural consistency.

### 3.3 Cloud Removal with Controlled Diffusion

**Conditional Control.** Following the principles of ControlNet [Zhang *et al.*, 2023a], we introduce a control variable  $\mathbf{c}$  to guide the diffusion process. The denoising process follows an iterative refinement step:

$$\mathbf{x}_{t+1} = \mathbf{x}_t - \gamma \nabla_{\mathbf{x}_t} \mathcal{L}_{\text{denoise}}(\mathbf{x}_t, \mathbf{c}), \quad (5)$$

where  $\mathbf{x}_t$  represents the image at time step  $t$ ,  $\mathbf{c}$  is the control signal,  $\gamma$  is the step size, and  $\mathcal{L}_{\text{denoise}}$  incorporates both cloud removal constraints and structure preservation.

**Grouped Learning.** To improve model adaptability, we employ grouped learning, combining  $k$ -means clustering with progressive training. Given training samples  $\mathcal{D} = \{(\mathbf{x}_i, \mathbf{y}_i)\}_{i=1}^N$ , we compute a similarity metric  $S_i$  based on SSIM and MSE:

$$S_i = \lambda_1 \cdot \text{MSE}(\mathbf{x}_i, \mathbf{y}_i) + \lambda_2 \cdot \text{SSIM}(\mathbf{x}_i, \mathbf{y}_i). \quad (6)$$

Samples are clustered into three groups,  $\mathcal{D}_1, \mathcal{D}_2, \mathcal{D}_3$ , based on increasing complexity, where complexity is determined by the similarity score  $S_i$ .

The detail of progressive training: We employ a three-stage progressive training strategy to improve model adaptability. The dataset is clustered into three groups  $\mathcal{D}_1, \mathcal{D}_2, \mathcal{D}_3$  based on increasing complexity. Training starts with simple cases in  $\mathcal{D}_1$  to learn basic transformations, then fine-tunes on moderate samples in  $\mathcal{D}_2$ , and finally refines on the most challenging cases in  $\mathcal{D}_3$ . At each stage  $t$ , the model updates as:

$$\theta_{t+1} = \theta_t - \eta \nabla_{\theta} \mathcal{L}(\mathcal{D}_t; \theta_t). \quad (7)$$

This gradual complexity increase stabilizes training, enhances generalization, and improves cloud removal accuracy.

### 3.4 Optimizing Image Quality and Modularization

**Feature Enhancement.** We integrate FreeU [Si *et al.*, 2024] to optimize feature representations by dynamically adjusting scaling and shifting parameters:

$$\mathbf{h}_{\text{scaled}} = s_1 \cdot \mathbf{h} + s_2, \quad \mathbf{h}_{\text{shifted}} = b_1 \cdot \mathbf{h}_{\text{scaled}} + b_2, \quad (8)$$

where  $\mathbf{h}$  is the feature map, and  $s_1, s_2, b_1, b_2$  are learnable parameters. This approach reduces artifacts, ensuring more realistic textures.

**Image Color Optimization.** We utilize a VGG-19 module with Gram matrix constraints [Gatys *et al.*, 2015] to enforce color consistency:

$$\mathcal{L}_{\text{style}} = \sum_l w_l \|G_l^{\text{gen}} - G_l^{\text{ref}}\|^2, \quad (9)$$

where  $G_l$  denotes Gram matrices computed from feature maps. This technique ensures harmonized color distributions across cloud-free images.

**Plug-and-Play Modular Design.** DC4CR adopts a modular design, allowing seamless integration into existing cloud removal frameworks. By incorporating LoRA, Grouped Learning, and Conditional Control, the model dynamically adjusts to diverse scenarios, ensuring both efficiency and accuracy.

## 4 Experiment

### 4.1 Dataset Description

To evaluate the efficiency of our proposed method, we utilize four datasets: RICE1/2 [Lin *et al.*, 2019] and CUHK-CR1/2 [Sui *et al.*, 2024]. The RICE dataset includes 500 images with thin cloud covers (RICE1) and 736 with thick cloud covers (RICE2). These images are randomly divided into an 80% training set and a 20% test set to ensure robust evaluation under various cloud conditions. Additionally, the CUHK-CR dataset comprises 1500 high-resolution images. The CUHK-CR dataset is further divided into CUHK-CR1 for thin clouds and CUHK-CR2 for thick clouds, facilitating a thorough assessment of our method’s effectiveness and robustness under varied imaging conditions.

---

### Algorithm 1 DC4CR: Cloud Removal via Diffusion Model

---

**Require:** Dataset  $\mathcal{D} = \{(\mathbf{x}_i, \mathbf{y}_i)\}_{i=1}^N$ , Pre-trained model  $\theta_0$   
**Ensure:** Fine-tuned model  $\theta$

- 1: Initialize  $\theta \leftarrow \theta_0$ , update LoRA  $\mathbf{A}, \mathbf{B}$
- 2: Compute  $S_i$  (SSIM + MSE), cluster into  $\mathcal{D}_1, \mathcal{D}_2, \mathcal{D}_3$  via  $k$ -means
- 3: **for**  $e = 1$  to  $N_{\text{epochs}}$  **do**
- 4:   **for**  $\mathcal{D}_t \in \{\mathcal{D}_1, \mathcal{D}_2, \mathcal{D}_3\}$  **do**
- 5:     **for** each  $(\mathbf{x}_i, \mathbf{y}_i) \in \mathcal{D}_t$  **do**
- 6:       Generate  $\mathbf{x}'_i = f_{\theta}(\mathbf{x}_i, p_i)$  with prompt  $p_i$
- 7:       Apply controlled diffusion:  $\mathbf{x}_{t+1} = \mathbf{x}_t - \gamma \nabla_{\mathbf{x}_t} \mathcal{L}_{\text{denoise}}(\mathbf{x}_t, \mathbf{c}_i)$
- 8:       Compute total loss:
- 9:        $\mathcal{L} = \lambda_1 \|\mathbf{x}_i - \mathbf{x}'_i\|^2 + \lambda_2 \text{SSIM}(\mathbf{x}_i, \mathbf{x}'_i) + \lambda_3 \mathcal{L}_{\text{style}}(\mathbf{x}'_i, \mathbf{y}_i)$
- 10:       Update latent embedding:  $\mathbf{z}_s^{(t+1)} = \mathbf{z}_s^{(t)} - \eta \nabla_{\mathbf{z}_s} \mathcal{L}$
- 11:     Apply FreeU enhancement:  $\mathbf{h}_{\text{shifted}} = b_1(s_1 \mathbf{h} + s_2) + b_2$
- 12:     Update  $\theta$  using Adam optimizer
- 13:   **end for**
- 14: **end for**
- 15: **end for**
- 16: **Return**  $\theta$

---

### 4.2 Implementation Details

All experiments were conducted on a single NVIDIA GeForce RTX 4090 GPU equipped with 24GB RAM, which provides high computational power and efficient processing capabilities, essential for handling large datasets and complex neural network operations. For the diffusion model generation stage, we used the pre-trained SD V1.5 with an instance prompt `remove <thin/thick> cloud`. The batch size was 4, and a learning rate of  $1 \times 10^{-4}$  using a constant rate scheduler, with training capped at 30,000 steps. In the condition control stage, we also used a learning rate of  $1 \times 10^{-4}$  without weight decay and a batch size of 4. The Adam optimizer ( $\beta_1=0.5, \beta_2=0.9$ ) was applied over 50 epochs, with Mean Squared Error (MSE) as the loss function.

### 4.3 Evaluation Metrics

To evaluate the performance, we use three metrics: Peak Signal-to-Noise Ratio (PSNR) [Hore and Ziou, 2010], Structural Similarity Index (SSIM) [Hore and Ziou, 2010], and Learned Perceptual Image Patch Similarity (LPIPS) [Zhang *et al.*, 2018]. These metrics assess both technical accuracy and perceptual quality. **PSNR** measures pixel-level fidelity, with higher values indicating better image quality. **SSIM** assesses structural similarity, with values from -1 to 1; higher values indicate greater similarity. **LPIPS** evaluates perceptual similarity using deep learning features; lower scores indicate higher similarity.

### 4.4 Comparison

We compare our DC4CR model with SOTA cloud removal methods, including SpA-GAN [Pan, 2020], AMGAN-CR [Xu *et al.*, 2022], CVAE [Ding *et al.*, 2022], MemoryNet

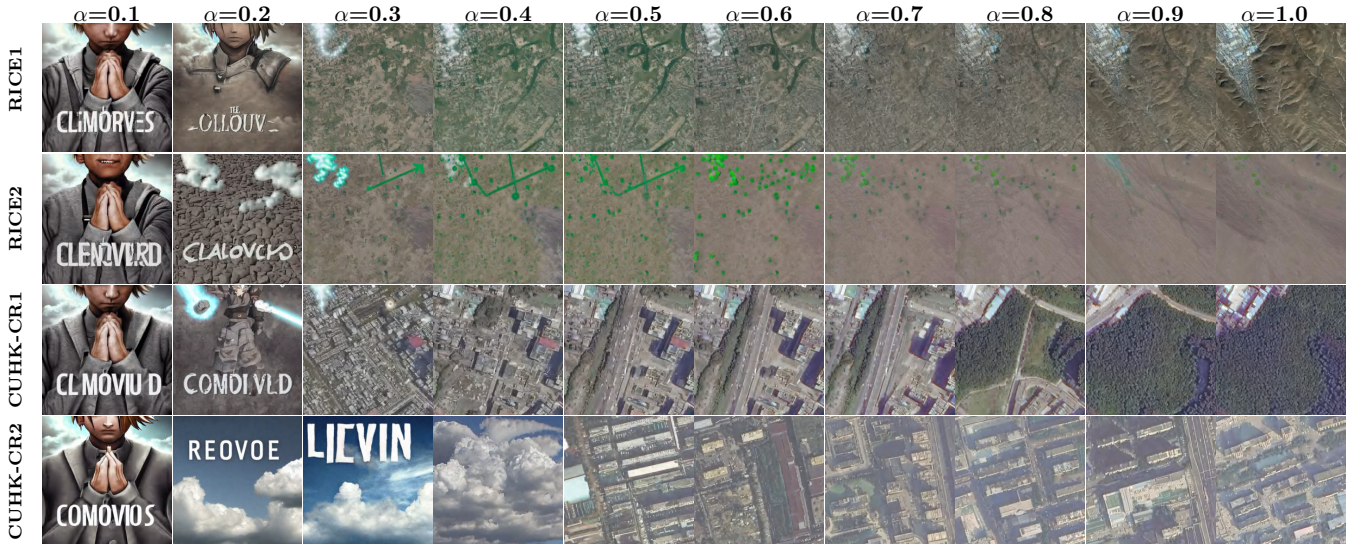


Figure 3: Comparison of weighting scaling factor  $\alpha$  settings. It demonstrates that  $\alpha \geq 0.5$  lead to better outcomes.

Table 3: Ablation results of the DC module. It analyses the impact of integrating the DC module into various reference models.

Method	DC	RICE1			RICE2			CUHK-CR1			CUHK-CR2		
		PSNR $\uparrow$	SSIM $\uparrow$	LPIPS $\downarrow$	PSNR $\uparrow$	SSIM $\uparrow$	LPIPS $\downarrow$	PSNR $\uparrow$	SSIM $\uparrow$	LPIPS $\downarrow$	PSNR $\uparrow$	SSIM $\uparrow$	LPIPS $\downarrow$
-	✓	35.542	0.9887	0.0054	33.678	0.8859	0.0451	26.291	0.7790	0.0285	24.595	0.6986	0.0326
MemoryNet	×	34.427	0.9865	0.0067	32.889	0.8801	0.0557	26.073	0.7741	0.0315	24.224	0.6838	0.0403
	✓	<b>35.715</b>	<b>0.9928</b>	<b>0.0050</b>	<b>33.796</b>	<b>0.8861</b>	<b>0.0450</b>	<b>26.633</b>	<b>0.8146</b>	<b>0.0252</b>	<b>24.805</b>	<b>0.7134</b>	<b>0.0302</b>
MSDA	×	34.569	0.9871	0.0073	33.166	0.8793	0.0463	25.435	0.7483	0.0374	23.755	0.6661	0.0433
	✓	<b>35.611</b>	<b>0.9893</b>	<b>0.0052</b>	<b>33.712</b>	<b>0.8899</b>	<b>0.0440</b>	<b>26.434</b>	<b>0.7908</b>	<b>0.0267</b>	<b>24.614</b>	<b>0.7043</b>	<b>0.0312</b>

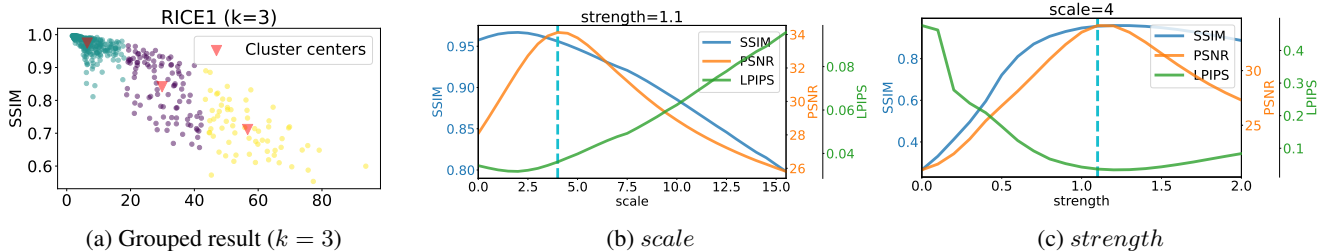


Figure 4: Grouped and controlling coefficients results. The optimal parameter values are  $scale = 4$  and  $strength = 1.1$ .

[Zhang *et al.*, 2023b], MSDA-CR [Yu *et al.*, 2022], DE-MemoryNet [Sui *et al.*, 2024], and DE-MSDA [Sui *et al.*, 2024]. The results are shown in Table 1, Figure 1, and Appendix.

As shown in Table 1, DC4CR achieves the highest PSNR (35.54 dB) and SSIM (0.9887) while obtaining the lowest LPIPS (0.0054) on RICE1, demonstrating superior image fidelity and perceptual quality. These improvements indicate better detail preservation and reduced artifacts compared to existing methods. Figure 1 illustrates that DC4CR effectively removes clouds while maintaining textures and structural details. Compared to DE-MemoryNet and DE-MSDA, our model produces cleaner reconstructions, especially in complex scenes with vegetation and urban areas.

DC4CR eliminates the need for pre-generated cloud masks, learning directly from cloud-covered images. The in-

tegration of enhancement parameters further refines feature extraction, improving adaptability to varying cloud conditions. Additionally, its prompt-driven control allows flexible cloud removal settings, enhancing practicality in remote sensing applications.

#### 4.5 Ablation Study

**Grouped Learning.** To evaluate the effectiveness of progressive learning, we applied  $k$ -means clustering ( $k = 2, 3$ ) to divide datasets into groups of increasing complexity. Appendix visualizes the clustering results, where samples are distributed based on SSIM and MSE. Table 5 quantifies the dataset partitioning, showing that a three-group division yields the best balance. Table 2 shows that the three-group setting consistently improves PSNR (by 0.5–1 dB) and SSIM while reducing LPIPS, especially in complex cloud cases.

Table 4: Weight scaling factor  $\alpha$  settings results. It indicates that  $\alpha = 0.7$  is the optimal setting, balancing performance and visual fidelity.

$\alpha$	RICE1			RICE2			CUHK-CR1			CUHK-CR2		
	PSNR $\uparrow$	SSIM $\uparrow$	LPIPS $\downarrow$	PSNR $\uparrow$	SSIM $\uparrow$	LPIPS $\downarrow$	PSNR $\uparrow$	SSIM $\uparrow$	LPIPS $\downarrow$	PSNR $\uparrow$	SSIM $\uparrow$	LPIPS $\downarrow$
0.1	21.340	0.5860	0.2123	18.378	0.4790	0.2960	13.337	0.4975	0.2490	12.282	0.4938	0.2531
0.3	25.934	0.7162	0.1408	22.980	0.6100	0.1732	19.181	0.5317	0.1453	19.869	0.5971	0.1430
0.5	33.437	0.9574	0.0096	31.125	0.7458	0.0654	25.257	0.6256	0.0380	23.588	0.6738	0.0392
0.6	34.390	0.9887	0.0073	32.771	0.8393	0.0510	25.872	0.7192	0.0285	23.987	0.6877	0.0336
0.7	<b>35.542</b>	<b>0.9887</b>	<b>0.0054</b>	<b>33.678</b>	<b>0.8859</b>	<b>0.0451</b>	<b>26.291</b>	<b>0.7790</b>	<b>0.0285</b>	<b>24.595</b>	<b>0.6986</b>	<b>0.0326</b>
0.8	35.435	0.9845	0.0061	33.676	0.8858	0.0456	26.288	0.7724	0.0292	24.592	0.6964	0.0333
0.9	35.441	0.9826	0.0063	33.674	0.8825	0.0458	26.285	0.7707	0.0293	24.586	0.6985	0.0331
1.0	35.229	0.9795	0.0057	33.669	0.8837	0.0451	26.286	0.7787	0.0294	24.593	0.6889	0.0335

Table 5:  $k$ -means clustering statistics of datasets. It summarizes the number of images in each group after applying  $k$ -means clustering. The result provides insights into the size of each cluster and help understand the contribution of different groups for training.

Group	RICE1			RICE2			CUHK-CR1			CUHK-CR2		
	Group-1	Group-2	Group-3	Group-1	Group-2	Group-3	Group-1	Group-2	Group-3	Group-1	Group-2	Group-3
No grouping	500	-	-	736	-	-	534	-	-	448	-	-
2 Groups	371	129	-	229	507	-	178	356	-	330	118	-
3 Groups	100	334	66	356	320	60	229	72	233	215	77	156

Without grouping, models struggle with diverse cloud conditions, confirming that progressive learning enhances stability and generalization.

**DC4CR Variants.** To assess the impact of our DC module, we integrated it into existing cloud removal models, specifically MemoryNet and MSDA. Figure 1 illustrates qualitative improvements in cloud removal performance, showing sharper textures and fewer artifacts compared to baseline models. Table 3 provides quantitative comparisons, where DC-MemoryNet achieves the highest PSNR and SSIM, outperforming DC-MSDA by 0.3 dB on average. Notably, on RICE2, DC-MemoryNet excels due to its superior handling of thick cloud occlusion, with a PSNR gain of 0.5 dB over DC-MSDA. These results validate the effectiveness of the DC module in enhancing cloud removal.

#### 4.6 Quantitative and Qualitative Analysis

**Weight Scaling Factor.** We investigated the effect of the weight scaling factor  $\alpha$  (ranging from 0 to 1) on image generation quality across different  $\alpha$  values. When  $\alpha < 0.3$ , the model is largely ineffective, especially on the CUHK-CR2 dataset, where  $\alpha < 0.5$  shows almost no effectiveness (Figure 3). At  $\alpha = 0.3$  and  $\alpha = 0.4$ , image quality is poor, with noticeable artifacts and distortions. However, with  $\alpha \geq 0.5$ , image quality begins to normalize, improving as  $\alpha$  increases, reaching peak performance at  $\alpha = 0.7$  (see Table 4). Beyond  $\alpha \geq 0.5$ , changes in evaluation metrics are minimal, indicating that  $\alpha$  directly influences image generation quality. While higher  $\alpha$  values yield clearer images, they may also distort land features, affecting the realism of the cloud removal effect. Therefore, selecting an appropriate  $\alpha$  is crucial for balancing quality and realism.

**Controlling Coefficients.** The *scale* parameter controls the prompt’s influence on content generation, while *strength* adjusts the intensity of conditioning input, affecting how closely the generated image matches the input conditions. Optimal settings of *scale* = 4 and *strength* = 1.1 (Fig-

ure 4) were identified, yielding the best image quality and accuracy. These findings highlight that proper parameter tuning significantly enhances model performance, aligning generated images more closely with expected outcomes. By adjusting *scale* and *strength*, we observed improved results across various tasks, allowing for better customization and optimization to meet specific application needs.

**Enhancement Parameters.** The parameter  $s$  adjusts feature amplitude through scaling, while  $b$  modifies feature translation via bias. Specifically,  $s_1$  and  $s_2$  scale features at different levels, and  $b_1$  and  $b_2$  adjust bias at specific levels. The parameters exhibit significant fluctuations based on the three evaluation metrics across the dataset (Figure Appendix). On the RICE1, the optimal parameter combination, relatively speaking, is  $s_1 = 0.9$ ,  $s_2 = 0.4$ ,  $b_1 = 1.1$ , and  $b_2 = 1.1$ . Using this parameter set achieves relatively good image quality and accuracy. This indicates that a suitable parameter setting is crucial for enhancing the performance of model. By comparing different parameter combinations, we observe that adjusting the  $s$  and  $b$  parameters significantly influences the feature representation of generated images, leading to better results in various tasks. Although there are fluctuations in the results, choosing appropriate parameters can effectively improve the model’s robustness and adaptability.

## 5 Conclusion

We propose **DC4CR**, a diffusion-based framework for cloud removal in remote sensing imagery. Our method eliminates the need for pre-generated cloud masks by leveraging prompt-driven control, enhancing preprocessing efficiency and adaptability. By integrating precise generation control and enhancement mechanisms, DC4CR achieves high-fidelity image restoration and state-of-the-art performance across multiple datasets. Additionally, our modular design allows seamless integration into existing cloud removal frameworks, further improving their effectiveness. These advance-

ments establish DC4CR as a powerful and flexible solution for remote sensing image processing.

## References

- Yong Chen, Wei He, Naoto Yokoya, and Ting-Zhu Huang. Blind cloud and cloud shadow removal of multitemporal images based on total variation regularized low-rank sparsity decomposition. *ISPRS Journal of Photogrammetry and Remote Sensing*, 157:93–107, 2019.
- Haidong Ding, Yue Zi, and Fengying Xie. Uncertainty-based thin cloud removal network via conditional variational autoencoders. In *Proceedings of the Asian Conference on Computer Vision*, pages 469–485, 2022.
- Patrick Ebel, Yajin Xu, Michael Schmitt, and Xiao Xiang Zhu. Sen12ms-cr-ts: A remote-sensing data set for multimodal multitemporal cloud removal. *IEEE Transactions on Geoscience and Remote Sensing*, 60:1–14, 2022.
- Leon Gatys, Alexander S Ecker, and Matthias Bethge. Texture synthesis using convolutional neural networks. *Advances in neural information processing systems*, 28, 2015.
- Jonathan Ho, Ajay Jain, and Pieter Abbeel. Denoising diffusion probabilistic models. *Advances in neural information processing systems*, 33:6840–6851, 2020.
- Jonathan Ho, Tim Salimans, Alexey Gritsenko, William Chan, Mohammad Norouzi, and David J Fleet. Video diffusion models. *Advances in Neural Information Processing Systems*, 35:8633–8646, 2022.
- Alain Hore and Djemel Ziou. Image quality metrics: Psnr vs. ssim. In *2010 20th international conference on pattern recognition*, pages 2366–2369. IEEE, 2010.
- Gensheng Hu, Xiaoyi Li, and Dong Liang. Thin cloud removal from remote sensing images using multidirectional dual tree complex wavelet transform and transfer least square support vector regression. *Journal of Applied Remote Sensing*, 9(1):095053–095053, 2015.
- Edward J Hu, Yelong Shen, Phillip Wallis, Zeyuan Allen-Zhu, Yuanzhi Li, Shean Wang, Lu Wang, and Weizhu Chen. Lora: Low-rank adaptation of large language models. *arXiv preprint arXiv:2106.09685*, 2021.
- James R Irons, John L Dwyer, and Julia A Barsi. The next landsat satellite: The landsat data continuity mission. *Remote sensing of environment*, 122:11–21, 2012.
- Shunping Ji, Peiyu Dai, Meng Lu, and Yongjun Zhang. Simultaneous cloud detection and removal from bitemporal remote sensing images using cascade convolutional neural networks. *IEEE Transactions on Geoscience and Remote Sensing*, 59(1):732–748, 2020.
- Bahjat Kawar, Shiran Zada, Oran Lang, Omer Tov, Huiwen Chang, Tali Dekel, Inbar Mosseri, and Michal Irani. Imagic: Text-based real image editing with diffusion models. In *Proceedings of the IEEE/CVF Conference on Computer Vision and Pattern Recognition*, pages 6007–6017, 2023.
- Xinghua Li, Huanfeng Shen, Liangpei Zhang, Hongyan Zhang, Qiangqiang Yuan, and Gang Yang. Recovering quantitative remote sensing products contaminated by thick clouds and shadows using multitemporal dictionary learning. *IEEE Transactions on Geoscience and Remote Sensing*, 52(11):7086–7098, 2014.
- Daoyu Lin, Guangluan Xu, Xiaoke Wang, Yang Wang, Xian Sun, and Kun Fu. A remote sensing image dataset for cloud removal. *arXiv preprint arXiv:1901.00600*, 2019.
- Heng Pan. Cloud removal for remote sensing imagery via spatial attention generative adversarial network. *arXiv preprint arXiv:2009.13015*, 2020.
- Robin Rombach, Andreas Blattmann, Dominik Lorenz, Patrick Esser, and Björn Ommer. High-resolution image synthesis with latent diffusion models. In *Proceedings of the IEEE/CVF conference on computer vision and pattern recognition*, pages 10684–10695, 2022.
- Natanuel Ruiz, Yuanzhen Li, Varun Jampani, Yael Pritch, Michael Rubinstein, and Kfir Aberman. Dreambooth: Fine tuning text-to-image diffusion models for subject-driven generation. In *Proceedings of the IEEE/CVF conference on computer vision and pattern recognition*, pages 22500–22510, 2023.
- Chitwan Saharia, William Chan, Saurabh Saxena, Lala Li, Jay Whang, Emily L Denton, Kamyar Ghasemipour, Raphael Gontijo Lopes, Burcu Karagol Ayan, Tim Salimans, et al. Photorealistic text-to-image diffusion models with deep language understanding. *Advances in neural information processing systems*, 35:36479–36494, 2022.
- Chenyang Si, Ziqi Huang, Yuming Jiang, and Ziwei Liu. Freeu: Free lunch in diffusion u-net. In *Proceedings of the IEEE/CVF Conference on Computer Vision and Pattern Recognition*, pages 4733–4743, 2024.
- Jialu Sui, Yiyang Ma, Wenhan Yang, Xiaokang Zhang, Man-On Pun, and Jiaying Liu. Diffusion enhancement for cloud removal in ultra-resolution remote sensing imagery. *IEEE Transactions on Geoscience and Remote Sensing*, 2024.
- Zixuan Tan, Jinnian Wang, Zhenyu Yu, and Yiyun Luo. Spatiotemporal analysis of xco2 and its relationship to urban and green areas of china’s major southern cities from remote sensing and wrf-chem modeling data from 2010 to 2019. *Geographies*, 3(2):246–267, 2023.
- Meilin Wang, Yexing Song, Pengxu Wei, Xiaoyu Xian, Yukai Shi, and Liang Lin. Idf-cr: Iterative diffusion process for divide-and-conquer cloud removal in remote-sensing images. *IEEE Transactions on Geoscience and Remote Sensing*, 2024.
- Pei Wang, Yun Yang, and Zhenyu Yu. Multi-batch nuclear-norm adversarial network for unsupervised domain adaptation. In *2024 IEEE International Conference on Multi-media and Expo (ICME)*, pages 1–6. IEEE, 2024.
- Meng Xu, Xiuping Jia, Mark Pickering, and Sen Jia. Thin cloud removal from optical remote sensing images using the noise-adjusted principal components transform. *ISPRS Journal of Photogrammetry and Remote Sensing*, 149:215–225, 2019.

- Meng Xu, Furong Deng, Sen Jia, Xiuping Jia, and Antonio J Plaza. Attention mechanism-based generative adversarial networks for cloud removal in landsat images. *Remote sensing of environment*, 271:112902, 2022.
- Ze Yang, Zhenyu Yu, Yuying Liang, Rui Guo, and Zhihua Xiang. Computer generated colorized image forgery detection using vlad encoding and svm. In *2020 IEEE 9th Joint International Information Technology and Artificial Intelligence Conference (ITAIC)*, volume 9, pages 272–279. IEEE, 2020.
- Tao Yang, Rongyuan Wu, Peiran Ren, Xuansong Xie, and Lei Zhang. Pixel-aware stable diffusion for realistic image super-resolution and personalized stylization. In *European Conference on Computer Vision*, pages 74–91. Springer, 2025.
- Zhenyu Yu and Chee Seng Chan. Yuan: Yielding unblemished aesthetics through a unified network for visual imperfections removal in generated images. *arXiv preprint arXiv:2501.08505*, 2025.
- Zhenyu Yu and Pei Wang. Capan: Class-aware prototypical adversarial networks for unsupervised domain adaptation. In *2024 IEEE International Conference on Multimedia and Expo (ICME)*, pages 1–6. IEEE, 2024.
- Weikang Yu, Xiaokang Zhang, and Man-On Pun. Cloud removal in optical remote sensing imagery using multiscale distortion-aware networks. *IEEE Geoscience and Remote Sensing Letters*, 19:1–5, 2022.
- Zhenyu Yu, Jinnian Wang, Zixuan Tan, and Yiyun Luo. Impact of climate change on sars-cov-2 epidemic in china. *Plos one*, 18(7):e0285179, 2023.
- Zhenyu Yu, Hua Wang, and Hanqing Chen. A guideline of u-net-based framework for precipitation estimates. *International Journal of Artificial Intelligence for Science (IJAI4S)*, 1(1), 2025.
- Zhenyu Yu, Jinnian Wang, Hanqing Chen, and Mohd Yamani Idna Idris. Qrs-trs: Style transfer-based image-to-image translation for carbon stock estimation in quantitative remote sensing. *IEEE Access*, 2025.
- Zhenyu Yu. Ai for science: A comprehensive review on innovations, challenges, and future directions. *International Journal of Artificial Intelligence for Science (IJAI4S)*, 1(1), 2025.
- Richard Zhang, Phillip Isola, Alexei A Efros, Eli Shechtman, and Oliver Wang. The unreasonable effectiveness of deep features as a perceptual metric. In *Proceedings of the IEEE conference on computer vision and pattern recognition*, pages 586–595, 2018.
- Lvmin Zhang, Anyi Rao, and Maneesh Agrawala. Adding conditional control to text-to-image diffusion models. In *Proceedings of the IEEE/CVF International Conference on Computer Vision*, pages 3836–3847, 2023.
- Xiao Feng Zhang, Chao Chen Gu, and Shan Ying Zhu. Memory augment is all you need for image restoration. *arXiv preprint arXiv:2309.01377*, 2023.
- Yue Zi, Fengying Xie, and Zhiguo Jiang. A cloud detection method for landsat 8 images based on pcanet. *Remote Sensing*, 10(6):877, 2018.